

Dedicated to Prof. Dorin N. Poenaru's  
70th Anniversary

## SYMMETRIC AND ASYMMETRIC SCISSION PROPERTIES IN THE FISSION OF PRE-ACTINIDES THROUGH HEAVY ACTINIDES

Y. NAGAME<sup>1</sup>, I. NISHINAKA<sup>1</sup>, Y.L. ZHAO<sup>2</sup>, H. NAKAHARA<sup>3</sup>

<sup>1</sup>*Advanced Science Research Center, Japan Atomic Energy Agency  
Tokai, Ibaraki 319-1195, Japan, E-mail: nagame.yuichiro@jaea.go.jp*

<sup>2</sup>*Institute of High Energy Physics, Chinese Academy of Sciences  
Beijing 100049, China*

<sup>3</sup>*Department of Chemistry, Tokyo Metropolitan University  
Hachioji, Tokyo 192-0397, Japan*

(Received February 23, 2007)

*Abstract.* Existence of two kinds of scission configurations associated with symmetric and asymmetric fission modes is pointed out in the fission of actinides: elongated and compact configurations. Each scission property is discussed in terms of shape elongation evaluated from fragment total kinetic energy (TKE). Fragment deformation at scission is also discussed based on neutron multiplicity measurements. From the systematic study of the scission properties in a wide range of actinides, the bimodal fission observed in the spontaneous fission (SF) of the heavy actinides would be interpreted as the result of the presence of the two fission paths; the ordinary asymmetric fission path is still existing while the symmetric one is bifurcated by strongly shell-influenced effects.

*Key words:* two-mode fission, symmetric fission, asymmetric fission, bimodal fission, scission configuration.

### 1. INTRODUCTION

The presence of two kinds of deformation paths in low energy fission of actinides was demonstrated by examining the correlation among saddle-point configurations, scission configurations and mass-yield distributions [1–3]. This is essentially experimental verification and further extension of the hypothesis of the two-mode fission by Turkevich and Niday [4]. The two deformation

paths are characterized as follows and schematically shown in Fig. 1. The first path is initiated at higher fission barrier and ends with an elongated scission configuration, giving a final mass yield centered around symmetric mass division, the symmetric fission path. In the second path, a fissioning nucleus experiences a lower fission barrier, resulting in a more compact scission configuration, which gives a double humped mass-yield distribution always centered around the heavy fragment mass number  $A = 140$ , the asymmetric fission path. The above picture has been well reproduced by the recent theoretical calculations of the potential energy surfaces by Möller *et al.* [6]; the saddle leading to the mass-symmetric division is found to be a few MeV higher than that to the mass-asymmetric division, and the compact scission configuration is related to the asymmetric fission and the elongated one associated with the symmetric fission path. A clear ridge separating the two fission valleys, symmetric and asymmetric, is also demonstrated [6]. (The presence of two static fission paths leading to different scission configurations separated by ridges was shown for the fission of actinides [7, 8].)

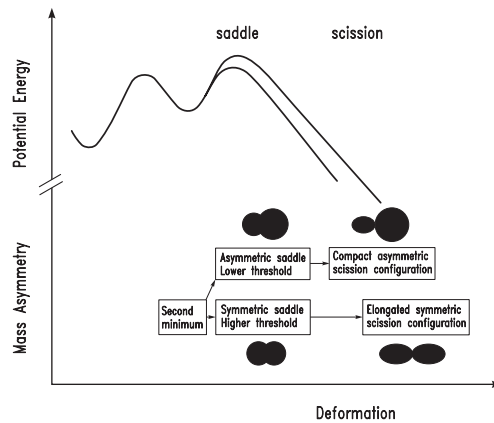


Fig. 1 – Schematic drawing of variation of the potential energy with deformation in the low energy fission of actinides. Taken from [5].

In this report, we summarize characteristics of the deformation properties of the symmetric and asymmetric scission configurations that are evaluated from experimental fragment total kinetic energy (TKE) and neutron multiplicity ( $\nu$ ), the number of neutrons emitted from fission fragments. Based on an extensive systematic analysis of deformation properties at scission in a wide range of fissioning nuclei, an interpretation of the so-called bimodal fission observed in the spontaneous fission (SF) of the heavy actinides is presented. The relationship between the scission properties in the fission of light actinides and those of the heavy actinides is briefly discussed.

## 2. TWO KINDS OF SCISSION CONFIGURATIONS

The existence of two distinctively different scission configurations for the same mass division was demonstrated in SF of the heavy actinides (*e.g.* [9,10]).

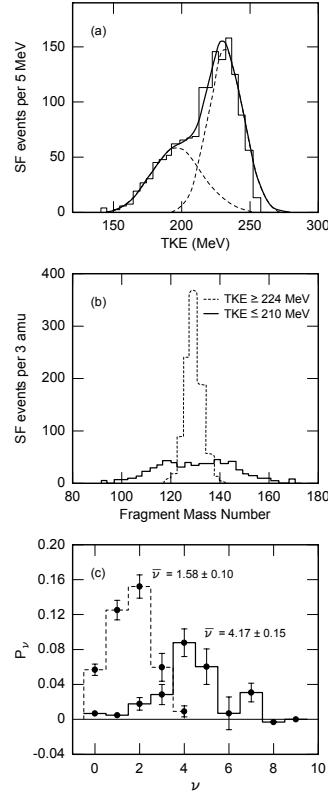


Fig. 2 – a) TKE distribution for spontaneous fission of  $^{260}\text{Md}$ . b) Decomposed mass-yield distributions for the events with  $\text{TKE} \geq 224$  MeV (dashed histogram) and for those with  $\text{TKE} \leq 210$  MeV (solid histogram). c) Neutron multiplicity distributions; the dashed histogram is derived from the events with  $\text{TKE} \geq 224$  MeV and the solid histogram is those from  $\text{TKE} \leq 210$  MeV. Taken from [11].

The most striking and significant features are that the mass-yield distribution is essentially single-peaked around the symmetric mass split, resulting in products with the mass number  $A \sim 130$ , whereas the TKE distribution apparently exhibits the structure with a shoulder that strongly suggests the presence of at least two components in the TKE distribution. As typical data, the TKE and mass-yield distributions observed in SF of  $^{260}\text{Md}$  [11] are depicted in Figs. 2(a) and 2(b), respectively; two components are clearly observed in the TKE distribution. The two component analysis yielded the fact

that the high-TKE events mostly constitute the sharp mass-yield curve around the symmetry and the low-TKE ones a broad flat-topped distribution. They also measured neutron multiplicity ( $\nu$ ) distributions in correlation with TKE of the fragments and observed a large drop in the number of neutrons emitted from the high-TKE component as shown in Fig. 2(c), implying that the fragments with the high-TKE component are less deformed while those with low-TKE are largely deformed at scission [11]. They called the fission with such phenomena bimodal fission.

Multimodal fission phenomena were also observed even in the light actinide fission. In the low energy proton-induced fission of Th through Cm, two components in the TKE distributions were verified by accurate measurements of velocities of complementary fragments in the fragment mass region around 130 where the asymmetric mass yield merges into the symmetric mass yield [1, 12, 13]. The two components were decomposed into low- and high-TKE ones. Assuming that TKE originates from the Coulomb repulsion energy between the two touching fragments at the scission point, the distance ( $D$ ) between the two charge centers of complementary fragments is evaluated from the average TKE value,  $\langle \text{TKE} \rangle$ .

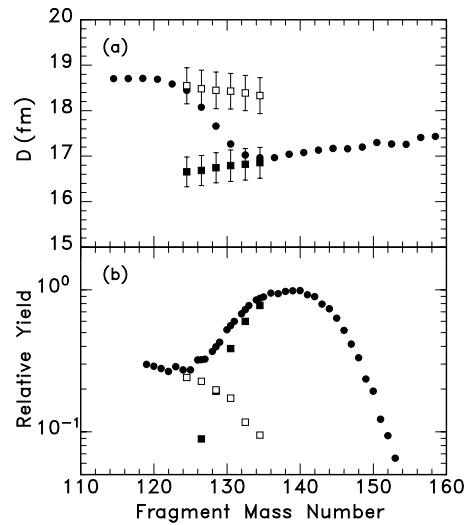


Fig. 3 – a) Distance between two charge centers at scission configurations evaluated from the average total kinetic energy  $\langle \text{TKE} \rangle$  of the fragment mass for the 13 MeV proton-induced fission of  $^{232}\text{Th}$ . Solid circles show the distance estimated from the  $\langle \text{TKE} \rangle$  values. Solid and open squares indicate the distances corresponding to the two types of average kinetic energies. b) Decomposed mass-yield curves. The solid and open squares are the decomposed mass yields corresponding to the high-TKE and low-TKE components, respectively. Adapted from [1].

The resulted  $D$ s are plotted in Fig. 3(a) as a function of heavy fragment mass number for the fission of 13-MeV proton-induced fission of  $^{232}\text{Th}$  [1]. The open and solid squares correspond to the distances obtained from the two-component analysis. It is clear that there are two kinds of scission configurations; the first one is the compact scission shape (small  $D$ ) and the other is the elongated one (large  $D$ ) in the fragment mass region around 130.

The intensity ratios of the two components in the TKE distributions were used to decompose the mass-yield distributions and the result is shown in Fig. 3(b). The open squares show the mass yields corresponding to the low-TKE components while the solid squares are those to high-TKE. The figure indicates that the overall mass yield curve is smoothly decomposed into two in the mass region  $A \sim 130$ . The correlation between the scission configurations and the mass-yield distributions reveals that the elongated scission configuration is associated with the mass-symmetric fission process while the compact scission configuration is with the mass-asymmetric one in the fission of the actinides [1, 12, 13].

### 3. FRAGMENT DEFORMATION AT SCISSION

Neutron multiplicity ( $\nu$ ) distributions well indicate the fragment deformation at scission as discussed in Section 2. The average neutron multiplicity ( $\bar{\nu}$ ) was measured in coincidence with fragments in the 12-MeV proton-induced fission of  $^{232}\text{Th}$  [14]. The  $\bar{\nu}$  values obtained for each fission mode are shown in Fig. 4 for the typical fragment pairs together with the TKE distributions. The left part shows  $\bar{\nu}$ s for the light fragments ( $A_L$ ) and the right ones are those for the complementary heavy fragments ( $A_H$ ). On the bottom left, those corresponding to the symmetrically divided products with  $A = 116 - 117$  are shown. For the typical asymmetric mass division,  $\bar{\nu}$ s of the light fragments with  $A_L = 88 - 89$  are considerably smaller than those of the complementary heavy fragments at the same TKE. This means that the heavy fragment has much excitation energy and deformed compared to the light fragments. The  $\bar{\nu}$  values of  $A_L = 102 - 103$  in the TKE region above 180 MeV (high TKE) become larger than those of the complementary heavy fragments ( $A_H = 130 - 131$ ), while  $\bar{\nu}$ s for the TKE below 170 MeV (low TKE) are smaller than those of  $A_H = 130 - 131$ . In the latter energy region,  $\bar{\nu}$  of the light fragment decreases as TKE becomes smaller whereas that of the heavy fragment rapidly increases. This indicates that in the fission events leading to high TKE, *i.e.*, the asymmetric fission mode, the fragments with  $A \sim 130$  are rather compact shaped while in those leading to low TKE, the symmetric fission mode, the corresponding fragments are largely deformed. On the

other hand, for the complementary light fragments with  $A_L = 102 - 103$ , no significant difference of  $\bar{\nu}$  is observed between the high-TKE and low-TKE components.

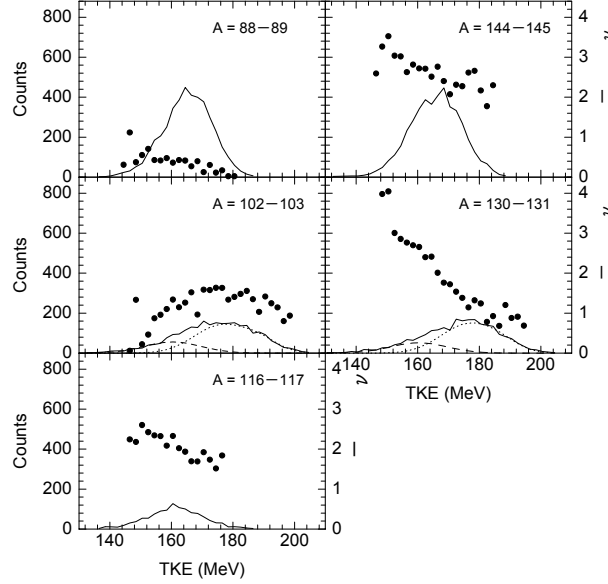


Fig. 4 – Average neutron multiplicity  $\bar{\nu}$  (solid circles) for the typical fragment pairs together with the TKE distributions in the 12-MeV proton-induced fission of  $^{232}\text{Th}$ . For the fragments with  $A = 102 - 103$  and  $130 - 131$ , the TKE distributions are decomposed into the low- and high-TKE components that are shown by dashed and dotted curves, respectively. Adapted from [14].

In Fig. 5, the  $\bar{\nu}$  values and those corresponding to the symmetric ( $\bar{\nu}_s$ ) and asymmetric ( $\bar{\nu}_a$ ) fission modes are shown as a function of fragment mass number by thick solid line, solid circles, and open circles, respectively. The decomposed mass-yield distributions for each symmetric and asymmetric fission are also depicted by dashed and dotted lines, respectively. The structure of  $\bar{\nu}$  at  $A_L \sim 100 - 110$  and  $A_H \sim 120 - 130$  is caused by the coexistence of the two fission modes. The so-called saw-tooth structure observed in low-energy fission of actinides is also seen in  $\bar{\nu}_a$  with the local minima at around  $A_L \sim 82$  and  $A_H \sim 130$  that correspond to the fragment shells of nuclei with  $N = 50$  and  $Z = 50$  ( $N = 82$ ) in the asymmetric fission, respectively. The  $\bar{\nu}_s$  value increases monotonously with the fragment mass number and becomes largely different from the value of  $\bar{\nu}_a$ . Based on these results, it is found that the different kinds of scission configurations associated with the symmetric and asymmetric fission modes are strongly affected by the different deformation

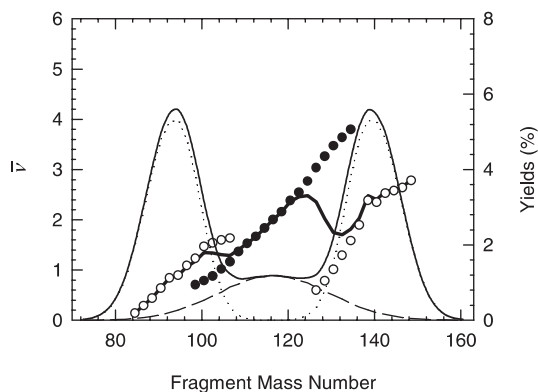


Fig. 5 – Average neutron multiplicity  $\bar{\nu}$  as a function of fragment mass number observed in the 12 MeV proton-induced fission of  $^{232}\text{Th}$ . Open circles correspond to the asymmetric fission mode and closed circles to the symmetric one. Mass-yield curve is decomposed into the symmetric and asymmetric distributions that are shown by dashed and dotted curves, respectively. Adapted from [14].

properties of the heavy fragments with the mass number  $A_H \sim 130$  compared with those of the complementary light fragments at  $A_L \sim 100$ . This means in the asymmetric fission mode the fragments show small deformation retaining closed shell effects, while in the symmetric fission the fragments are largely deformed.

#### 4. DEGREE OF FRAGMENT DEFORMATION AT SCISSION

We discuss the systematic variation of the elongated and compact scission configurations in terms of shape elongation evaluated from the experimental TKE values including a large number of literature data (see [13, 15]). The shape elongation parameter  $\beta$  which reflects the degree of deformation at scission is defined as  $\beta = D/D_0$ , where  $D_0$  indicates the distance between charge centers of two touching spheres. The distance  $D$  is evaluated from  $\langle \text{TKE} \rangle$  as described in Section 3.

The  $\beta_{asym}$  values for the scission configurations leading to the asymmetric mass division that produce the typical heavier fragment mass of  $A_H = 140$  are plotted in Fig. 6(a) as a function of the mass number of the fissioning nuclei  $A_f$ . It is found that  $\beta_{asym}$  shows nearly the same value of 1.53 for both the particle-induced fission and SF, indicating that the degree of deformation at scission for the asymmetric fission mode is independent of the excitation energy ( $E^*$ ) of the fissioning nucleus. It is also interesting to note that the  $\beta_{asym}$  values evaluated from the low-TKE component in the bimodal fission

(closed squares) are equal to those in the pre-actinide and actinide region. The ordinary asymmetric fission mode passing through the asymmetric valley is evidently present even in the heavy actinide region. As shown in Fig. 2(b), the fragments with low TKE seems to constitute the asymmetric mass distribution which has peaks around  $A_L \sim 120$  and  $A_H \sim 140$ .

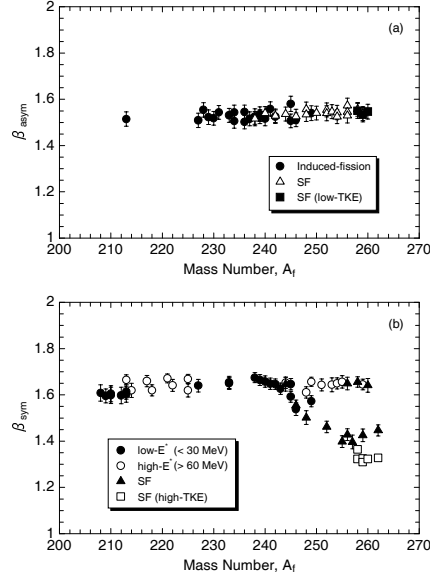


Fig. 6 – a) Shape elongation at scission for the asymmetric mass division as a function of the mass number of the fissioning nuclei  $A_f$ . Solid circles are results corresponding to the particle-induced fission while open triangles are for spontaneous fission. Solid squares are those corresponding to the low-TKE component observed in the bimodal fission of the heavy actinides. b) Shape elongation for symmetric mass division as a function of  $A_f$ . Solid circles are the results for the low excitation fission ( $E^* < 30$  MeV), while open circles are those for the high excitation fission ( $E^* > 65$  MeV). Solid triangles are for SF corresponding to the symmetric mass division of the high-TKE component in Fig. 2(b) and open squares show the results of the high-TKE component observed in the bimodal fission of the heavy actinide region. Adapted from [13, 15].

Figure 6(b) shows the  $\beta_{sym}$  values evaluated from the  $\langle TKE \rangle$  data for the symmetric mass division of  $A_1 = A_2 = A_f/2$ . It is clear that the two extreme types of  $\beta_{sym}$  are present. The one is for the low- $E^*$  fission in the region from the pre-actinide through the actinide until  $A_f \sim 245$  (solid circles) and for the high- $E^*$  fission (open circles) in a wide range of  $A_f$ , where  $\beta_{sym}$  is nearly a constant of 1.65. The other type of behavior is for SF in the region of  $A_f \sim 260$ , at which  $\beta_{sym}$  is decreased to a constant value of 1.33 (open squares) which corresponds to that evaluated from the high-TKE component

in the bimodal fission. The implied smaller elongation at scission would be related to the effects of spherical fragment shells of  $Z = 50$  and  $N = 82$  on the mass-symmetric deformation. Note that  $\beta_{sym}$  in the low- $E^*$  fission and SF gradually becomes smaller beyond  $A_f = 245$  approaching the value of 1.33; the shell effects on the scission shape in the symmetric fission valley are gradually manifested as a function of the neutron and atomic numbers of the fissioning nuclei, although such effects do not appear in the fission that goes through the deformation path in the asymmetric fission valley. It is also found that due to washing out of shell effects in hot nuclei,  $\beta_{sym}$  in the high- $E^*$  fission observed in  $A_f \geq 245$  keeps the value of 1.65. However, there are also some SF data,  $^{256,258,260}\text{Rf}$  ( $N = 152, 154, 156$ ) [16], even in  $A_f \geq 245$  that show  $\beta_{sym} = 1.65$ . At the extremely high TKE or very small  $\beta_{sym}$ , the sudden variation of the mass-yield curves to the symmetric narrow shape are obvious for the fissioning nuclei with the atomic number around 100 and the neutron number 160 [15]. Thus the above features in SF would be explained by that the neutron number of those fissioning nuclei is not close enough to  $N = 160$ . The  $\beta_{sym}$  values (solid triangles) located in between  $\beta_{sym} = 1.65$  and  $\beta_{sym} = 1.33$  around  $A_f = 260$  may be interpreted as the mixture of the high- and low-TKE components (no clear two components in the TKE distributions were observed in SF of  $^{259}\text{Lr}$  [17] and  $^{262}\text{Rf}$  [18]).

The systematic features of the  $\beta$  values in the fission of actinides have been well reproduced by the theoretical calculations based on the two-center shell model coupling with the dynamical calculations using the multi-dimensional Langevin equation [19]. Three types of the scission configurations in the fission of  $^{264}\text{Fm}$  were pointed out as follows: mass-symmetric compact configuration, mass-asymmetric configuration, and mass-symmetric elongated configuration [19]. Further they calculated the mass-yield and TKE distributions for each type of the scission configurations. Recently, dynamical effects including the dissipation tensor have been taken into account to calculate the mass-yield and TKE distributions in each deformation [20].

The average TKEs observed in various fission systems are approximately expressed in terms of the Coulomb parameter,  $Z_f^2/A_f^{1/3}$ , where  $Z_f$  indicates the atomic number of fissioning nuclei. It is known that the formula proposed by Viola *et al.* [21] works very well to reproduce the experimental data for both of the symmetric and asymmetric fission. Based on the constant  $\beta$  values as discussed,  $\beta_{sym} = 1.65$  and  $\beta_{asym} = 1.53$ , the new empirical formula have been derived for the TKE release in the fission process:

$$\langle \text{TKE} \rangle_{\text{sym}} = 0.1173 \times Z_f^2/A_f^{1/3} + 7.5 \text{MeV} \quad (1)$$

for the symmetric fission and

$$\langle \text{TKE} \rangle_{\text{asym}} = 0.1217 \times Z_f^2/A_f^{1/3} + 3.5 \text{MeV} \quad (2)$$

for the asymmetric one [15].

## 5. BIMODAL FISSION IN HEAVY ACTINIDES

According to the calculations of fission paths on multi-dimensional potential energy surfaces [22], two main paths are given after passing through a single barrier (no second hump of the barrier) for the fission of  $^{258}\text{Fm}$ ; one proceeds to a symmetric valley with a compact shape of the scission configuration and the other to an asymmetric valley with an elongated shape at scission as shown in Fig. 7(a).

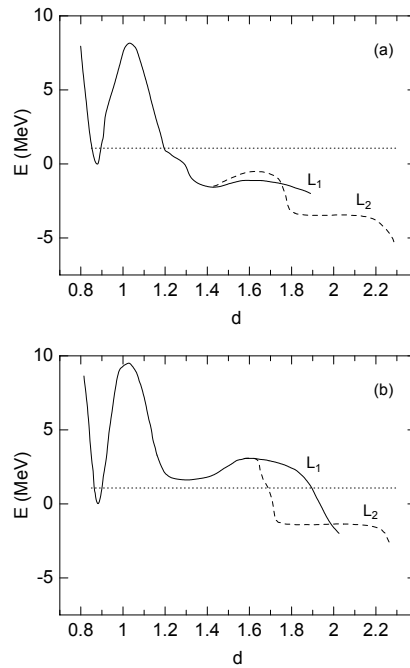


Fig. 7 – Fission barriers along the trajectories for: a)  $^{258}\text{Fm}$ ; b)  $^{254}\text{Fm}$ .  $L_1$  and  $L_2$  denote the trajectories corresponding to the symmetric and asymmetric fission valleys. The parameter  $d$  indicates  $r/R_0$ , which is the distance  $r$  between the mass center of the fission fragments divided by the equivalent spherical radius  $R_0$  of the nucleus.  $d$  is almost equivalent to  $\beta$  defined in [13, 15]. Taken from [22].

The calculation succeeds in explaining the feature of the bimodal fission in which two types of fission events corresponding to the compact and elongated scission shapes are present with comparable yields. A similar calculation was conducted for the fission of  $^{254}\text{Fm}$  and two paths with different thicknesses of the second barrier are presented as shown in Fig. 7(b); the path leading to

the symmetric fission valley has a thicker barrier to penetrate and reaches scission with a less compact shape compared to the one in  $^{258}\text{Fm}$ , and the other path leading to the asymmetric fission valley has a thinner barrier and ends with an elongated scission shape. The result is consistent with the experimental observation of a double-humped asymmetric mass-yield distribution for SF of  $^{254}\text{Fm}$  [23].

The recent calculations by Möller *et al.* [6] show the presence of different saddle point configurations for each deformation path to the symmetric and asymmetric fission valleys in the Fm region. It is interesting to note that the relative heights of the symmetric and the asymmetric barriers are reversed when the neutron number is increased by two units; the saddle leading to the asymmetric valley is lower in the fission of  $^{256}\text{Fm}$  whereas it becomes higher than the one leading to the symmetric valley in  $^{258}\text{Fm}$ . Thus, there exists a transition point in the height of the saddle from the asymmetric to the symmetric in this region with neutron number around 160. The theoretical results reproduce the systematic change of the mass-yield distributions in SF summarized by Hoffman *et al.* [24, 25].

These calculations are also in conformity with the experimental results observed in the thermal-neutron-induced fission of  $^{255}\text{Fm}$  [26] and  $^{257}\text{Fm}$  [27]. In the former, a broad symmetric mass-yield curve is observed while in the latter, the contribution of the asymmetric mass-yields becomes more conspicuous. As pointed out by Hoffman *et al.* [28], in the case of SF of  $^{256}\text{Fm}$ , the fragment shell effects tend to stabilize asymmetric mass division, while in SF of  $^{258}\text{Fm}$ ,  $^{259}\text{Fm}$  and other neutron-rich heavy actinides with  $N \sim 160$  they stabilize symmetric mass division. They also suggested that the heavy Fm region is a transition region where competing fission modes can have substantial yields [29]. These pictures fairly reproduce the experimental results (Fig. 8) summarized by Britt *et al.* [29].

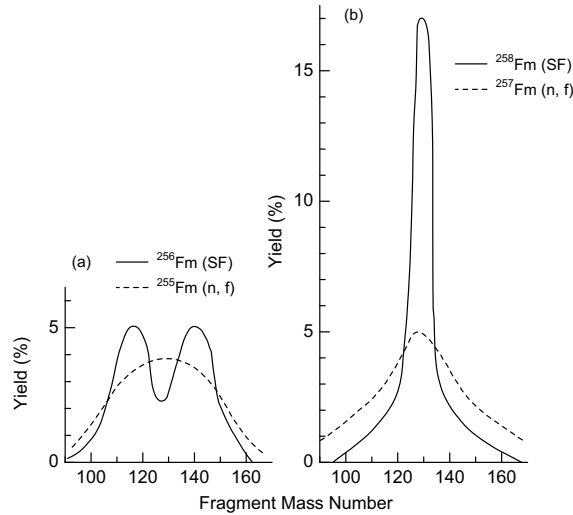


Fig. 8 – Provisional mass-yield distributions for: a)  $^{256}\text{Fm}$  (SF) and  $^{255}\text{Fm}(n, f)$ ; b)  $^{258}\text{Fm}$  (SF) and  $^{257}\text{Fm}(n, f)$ . Taken from [29].

From the systematic features of the shape elongation at scission and the mass-yield distributions, the following remarks are also worthwhile. As the barrier penetration phenomena in SF are so sensitively dependent on the height and shape of the fission barriers, the effects of nuclear shell structure of the fissioning nuclei and/or of the fragments are dramatically evident in the observed mass-yield curves; they suddenly change from the ordinary double humped one to a single narrow one by an addition of one neutron to the fissioning nucleus.

It is also worth pointing out that in the fission of superheavy nuclei with  $A_f \sim 280$ , the two fission valleys, symmetric and asymmetric, may merge into one, due to the mass symmetry leading to the fragments  $A \sim 140$  which is affected by the deformed shells ( $N = 88$ ) as observed in the ordinary asymmetric fission [30]. Thus, a mass distribution with a single peak at  $A \sim 140$  and with the most probable TKE around 240 – 250 MeV evaluated from the constancy of  $\beta_{asym}$  would be expected.

## 6. CONCLUSIONS

The two kinds of scission configurations, compact and elongated, in the actinide fission was presented. The different scission configurations associated with the two fission modes were found to originate from extremely different degrees of the fragment deformation at the fragment mass number  $A \sim 130$ . From the extensive systematic study of the deformation of scission configurations, it was shown that there were three types of shape elongation at the scission: the ordinary mass-asymmetric deformation, the liquid-drop property governed mass-symmetric deformation, and the shell-influenced mass-symmetric deformation. It was also found that the asymmetric fission path still exists even in the bimodal fission of the heavy actinides, while the shell influenced symmetric fission path is gradually manifested in SF of the heavy actinides.

*Acknowledgements.* Y. N. is grateful to Dorin N. Poenaru for fruitful and valuable discussions on the shape of the scission configurations.

## REFERENCES

1. Y. Nagame, I. Nishinaka, K. Tsukada, Y. Oura, S. Ichikawa, H. Ikezoe, Y.L. Zhao, K. Sueki, H. Nakahara, M. Tanikawa, T. Ohtsuki, H. Kudo, Y. Hamajima, K. Takamiya and Y.H. Chung, Phys. Lett., **B387**, 26 (1996).

2. Y. Nagame, I. Nishinaka, K. Tsukada, S. Ichikawa, H. Ikezoe, Y.L. Zhao, Y. Oura, K. Sueki, H. Nakahara, M. Tanikawa, T. Ohtsuki, K. Takamiya, K. Nakanishi, H. Kudo, Y. Hamajima and Y.H. Chung, *Radiochim. Acta*, **78**, 3 (1997).
3. T. Ohtsuki, Y. Nagame and H. Nakahara, *Bimodal nature of nuclear fission*, in *Heavy Elements and Related New Phenomena*, Vol. 1, edited by W. Greiner and R.J. Gupta, World Scientific, Singapore, 1999.
4. A. Turkevich and J. B. Niday, *Phys. Rev.*, **84**, 52 (1951).
5. Y. Nagame, Y.L. Zhao, I. Nishinaka, S. Goto, D. Kaji, M. Tanikawa, K. Tsukada, M. Asai, H. Haba, M. Sakama, S. Ichikawa, K. Sueki, H. Kudo and H. Nakahara, *Radiochim. Acta*, **89**, 681 (2001).
6. P. Möller, D.G. Madland, A.J. Sierk and A. Iwamoto, *Nature (London)*, **409**, 785 (2001).
7. V.V. Pashkevich, *Nucl. Phys.*, **A169**, 275 (1971).
8. U. Brosa, S. Grossmann and A. Müller, *Phys. Rep.*, **197**, 167 (1990).
9. E.K. Hulet, J.F. Wild, R.J. Dougan, R.W. Lougheed, J.H. Landrum, A.D. Dougan, M. Schädel, R.L. Hahn, P.A. Baisden, C.M. Henderson, R.J. Dupzyk, K. Sümmerer and G.R. Bethune, *Phys. Rev. Lett.*, **56**, 313 (1986).
10. E.K. Hulet, J.F. Wild, R.J. Dougan, R.W. Lougheed, J.H. Landrum, A.D. Dougan, P.A. Baisden, C.M. Henderson, R.J. Dupzyk, R.L. Hahn, M. Schädel, K. Sümmerer and G.R. Bethune, *Phys. Rev.*, **C 40**, 770 (1989).
11. J.F. Wild, J. van Aarle, W. Westmeier, R. Lougheed, E.K. Hulet, K.J. Moody, R.J. Dougan, E.-A. Koop, R.E. Glaser, R. Brandt and P. Patzelt, *Phys. Rev.*, **C 41**, 640 (1990).
12. T. Ohtsuki, Y. Nagame, H. Ikezoe, K. Tsukada, K. Sueki and H. Nakahara, *Phys. Rev. Lett.*, **66**, 17 (1991).
13. Y.L. Zhao, I. Nishinaka, Y. Nagame, M. Tanikawa, K. Tsukada, S. Ichikawa, K. Sueki, Y. Oura, H. Ikezoe, S. Mitsuoka, H. Kudo and H. Nakahara, *Phys. Rev. Lett.*, **82**, 3408 (1999).
14. I. Nishinaka, Y. Nagame, H. Ikezoe, M. Tanikawa, Y.L. Zhao, K. Sueki and H. Nakahara, *Phys. Rev.*, **C 70**, 014609 (2004).
15. Y.L. Zhao, Y. Nagame, I. Nishinaka, K. Sueki and H. Nakahara, *Phys. Rev.*, **C 62**, 014612 (2000).
16. E.K. Hulet, *Phys. Atom. Nucl.*, **57**, 1165 (1994).
17. T.M. Hamilton, K.E. Gregorich, D.M. Lee, K.R. Czerwinski, N.J. Hannink, C.D. Kacher, B. Kadkhodayan, S.A. Kreek, M.J. Nurmi, M.R. Lane, M.P. Neu, A. Türler and D.C. Hoffman, *Phys. Rev.*, **C 46**, 1873 (1992).
18. M.R. Lane, K.E. Gregorich, D.M. Lee, M.F. Mohar, M. Hsu, C.D. Kacher, B. Kadkhodayan, M.P. Neu, N.J. Stoyer, E.R. Sylwester, J.C. Yang and D.C. Hoffman, *Phys. Rev.*, **C 53**, 2893 (1996).
19. T. Asano, T. Wada, M. Ohta, T. Ichikawa, S. Yamaji and H. Nakahara, *J. Nucl. Radiochem. Sci.*, **5**, 1 (2004).
20. T. Asano, T. Wada, M. Ohta, S. Yamaji and H. Nakahara, *J. Nucl. Radiochem. Sci.*, **7**, 7 (2006).
21. V.E. Viola, K. Kwiatkowski and M. Walker, *Phys. Rev.*, **C 31**, 1550 (1985).
22. S. Ćwiok, P. Rozmej, A. Sobczewski and Z. Patyk, *Nucl. Phys.*, **A 491**, 281 (1989).
23. J.E. Gindler, K.F. Flynn, L.E. Glendenin and R.K. Sjoblom, *Phys. Rev.*, **C 16**, 1483 (1977).
24. D. C. Hoffman and M. R. Lane, *Radiochim. Acta*, **70/71**, 135 (1995).
25. D.C. Hoffman, T.M. Hamilton and M.R. Lane, *Spontaneous Fission*, in *Nuclear Decay Modes*, edited by D. N. Poenaru, Institute of Physics Publishing, Bristol, 1996.

- 
26. R.C. Ragaini, E.K. Hulet, R.W. Lougheed and J. Wild, *Phys. Rev., C* **9**, 399 (1974).
  27. W. John, E.K. Hulet, R.W. Lougheed and J.J. Wesolowski, *Phys. Rev. Lett.*, **27**, 45 (1971).
  28. D.C. Hoffman, J.B. Wilhelmy, J. Weber, W.R. Daniels, E.K. Hulet, R.W. Lougheed, J.H. Landrum, J.F. Wild and R.J. Dupzyk, *Phys. Rev., C* **21**, 972 (1980).
  29. H.C. Britt, D.C. Hoffman, J. van der Plicht, J.B. Wilhelmy, E. Cheifetz, R.J. Dupzyk and R.W. Lougheed, *Phys. Rev., C* **30**, 559 (1984).
  30. B.D. Wilkins, E.P. Steiberg and R.R. Chasman, *Phys. Rev., C* **14**, 1832 (1976).